

# Estimating Maximum Surface Winds from Hurricane Reconnaissance Measurements

MARK D. POWELL AND ERIC W. UHLHORN

*NOAA/Atlantic Oceanographic and Meteorological Laboratory/Hurricane Research Division, Miami, Florida*

JEFFREY D. KEPERT

*Centre for Australian Weather and Climate Research, Bureau of Meteorology, Melbourne, Victoria, Australia*

(Manuscript received 2 November 2007, in final form 19 October 2008)

## ABSTRACT

Radial profiles of surface winds measured by the Stepped Frequency Microwave Radiometer (SFMR) are compared to radial profiles of flight-level winds to determine the slant ratio of the maximum surface wind speed to the maximum flight-level wind speed, for flight altitude ranges of 2–4 km. The radius of maximum surface wind is found on average to be 0.875 of the radius of the maximum flight-level wind, and very few cases have a surface wind maximum at greater radius than the flight-level maximum. The mean slant reduction factor is 0.84 with a standard deviation of 0.09 and varies with storm-relative azimuth from a maximum of 0.89 on the left side of the storm to a minimum of 0.79 on the right side. Larger slant reduction factors are found in small storms with large values of inertial stability and small values of relative angular momentum at the flight-level radius of maximum wind, which is consistent with Kepert's recent boundary layer theories. The global positioning system (GPS) dropwindsonde-based reduction factors that are assessed using this new dataset have a high bias and substantially larger RMS errors than the new technique. A new regression model for the slant reduction factor based upon SFMR data is presented, and used to make retrospective estimates of maximum surface wind speeds for significant Atlantic basin storms, including Hurricanes Allen (1980), Gilbert (1988), Hugo (1989), Andrew (1992), and Mitch (1998).

## 1. Introduction

Motivated by the difficulty of obtaining measurements of the peak surface wind in hurricanes, several methods have been formulated to estimate surface winds from flight-level reconnaissance wind measurements (e.g., Powell 1980; Powell and Black 1990; Franklin et al. 2003; Dunion et al. 2003). Aircraft flight levels near 3 km are of particular interest since that altitude is typically flown in mature hurricanes and is too high to directly invoke boundary layer models (Powell et al. 1999). The aforementioned papers focused on reduction factors ( $F_r$ ) based on the ratio of the surface wind to the flight-level wind speed, with the surface wind either directly below the location of the flight-level wind measurement, or along the sloping global positioning system dropwindsonde (GPS sonde) trajectory, the inward dis-

placement of which is normally substantially less than the eyewall slope.<sup>1</sup> A summary of the vertical and slant reduction factor terminology to be used in this paper is included in Table 1. A transect of simultaneous 10-m and flight-level wind speeds through Hurricane Katrina is shown in Fig. 1, in which the surface radii of maximum winds ( $R_{mxs}$ ) are each located 5–6 km inward of the corresponding flight-level radii of maximum winds ( $R_{mxf}$ ). This outward slope of the radius of maximum wind ( $R_{MW}$ ) with height results in very large radial gradients of  $F_r$  near the  $R_{MW}$ , with the risk of significant errors in estimates of the operationally important maximum surface wind speed ( $V_{mxs}$ ). Indeed, these data imply that (i) estimating the surface wind directly beneath a flight-level estimate and (ii) estimating the

---

Corresponding author address: Dr. Mark Powell, FSU-COAPS, 2035 E. Paul Dirac Dr., 200 RM Johnson Bldg., Tallahassee, FL 32306-2840.  
E-mail: mark.powell@noaa.gov

---

<sup>1</sup> Although the maximum inflow speed can reach 2–3 times the GPS sonde fall speed of  $12 \text{ m s}^{-1}$ , the maximum inflow occurs in a thin layer near the surface, and thus leads to only a modest inward displacement of the GPS sonde. Even in intense storms, the inward displacement of a GPS sonde trajectory is small; see, for example, Kepert (2006a, Fig. 4).

TABLE 1. Definitions of symbols used in the text.

Quantity	Description
$V_f, V_{mxf}, R_{mxf}$	Flight-level wind speed, maximum flight-level wind speed, and its radius along a radial flight leg
$V_s, V_{mxs}, R_{mxs}$	Surface wind speed, maximum surface wind speed, and its radius along a radial flight leg
$F_r$	Vertical reduction factor: $V_s/V_f$
$F_{rmx}$	Slant reduction factor: $V_{mxs}/V_{mxf}$
$F_{rmxl}$	$V_{mxs}/V_{mxf}$ for $V_{mxs}$ obtained in radial leg containing the largest $V_{mxf}$ for the mission
$F_{rmxa}$	$V_{mxs}/V_{mxf}$ for the largest $V_{mxs}$ and $V_{mxf}$ anywhere in the storm over the course of a mission regardless of radial leg
$R_{mxs}/R_{mxf}$	Relative slope of the radius of the maximum wind
$R_{MW}$	Radius of maximum wind as a function of height

maximum surface wind in the vicinity of a measured flight-level wind maximum should be regarded as distinct problems.

Two causes for the outward slope of the  $R_{MW}$  with height are illustrated in the schematic in Fig. 2. It has long been known (e.g., Shaw 1922; Haurwitz 1935) that the baroclinic warm core structure of the tropical cyclone leads to a decrease in the vortex strength with height (Fig. 2a), and an outward tilt of angular momentum

surfaces ( $M$ ) with height (Fig. 2b), while the  $R_{MW}$  above the boundary layer is to good approximation a constant  $M$  surface. The magnitude of  $R_{MW}$  tilt is greatest in the upper troposphere, where the warm core is strongest. The second cause of  $R_{MW}$  tilt is surface friction, which produces a significant inward displacement of the  $R_{MW}$  in the lowest 500 m to 1 km (Kepert 2001; Kepert and Wang 2001). This lower portion of the  $R_{MW}$  does not follow an  $M$  surface, since this slopes inward with increasing height

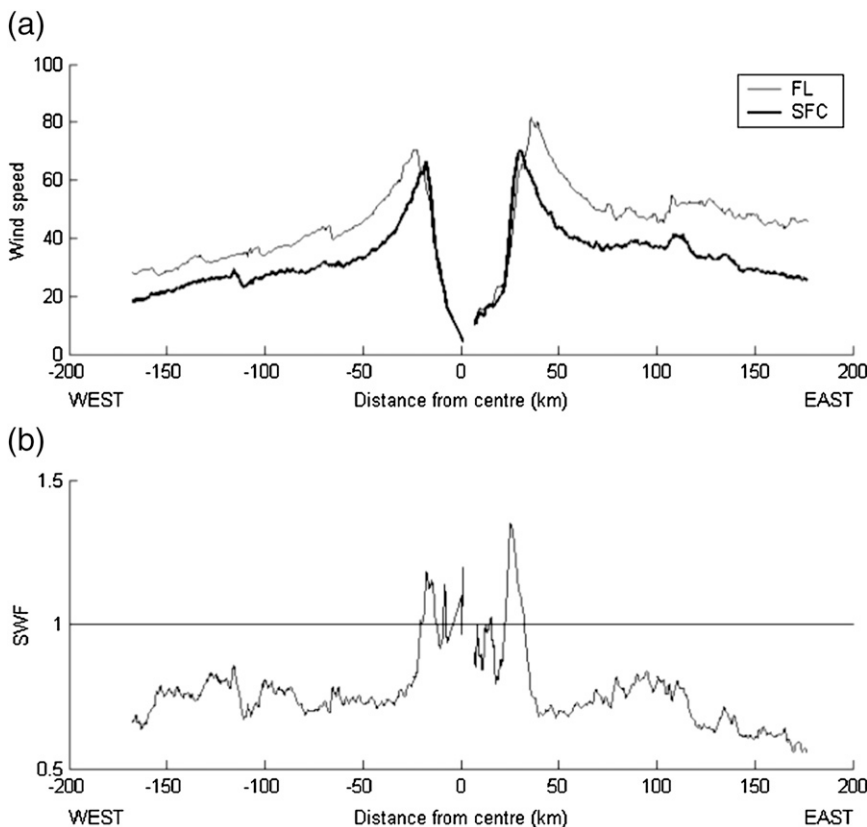


FIG. 1. (a) Observed SFMR surface (heavy) and flight-level (3 km, light) wind speeds from a research aircraft transect through Hurricane Katrina commencing at 1708 UTC 28 Aug 2005. Katrina was moving northward at the time, so west is to the left of the track. The small amount of missing data near the storm center is due to the aircraft’s maneuvering. (b) Ratio of the surface wind to the flight-level wind at the same radius derived from the data in (a); note the very large gradient of  $F_r$  between the surface and flight-level radii of maximum winds.

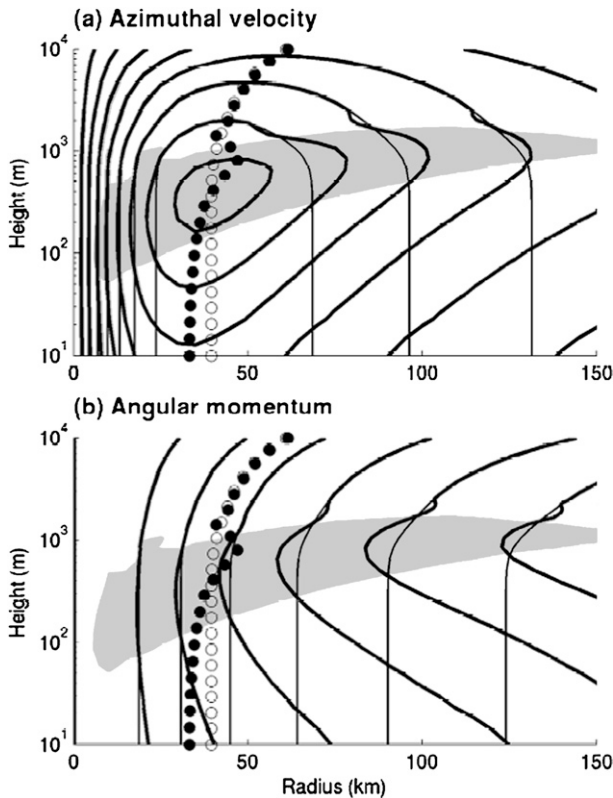


FIG. 2. Schematic adapted from Kepert and Wang (2001, Fig. 2), showing the processes that lead to the tilt of the  $R_{MW}$  in a hurricane. (a) Radius–height section of gradient wind speed (thin contours) and the azimuthal wind component (thick contours) in a hurricane. The gray shading shows the region of supergradient winds near the boundary layer top, and the filled (open) circles show the radius of the maximum (gradient) wind, which slopes outward with height above the boundary layer due to the warm core, and within most of the boundary layer due to frictional dynamics. (b) Similar to (a) but showing angular momentum with (thick lines) and without (thin lines) the influence of friction. Note that in the absence of friction, the  $R_{MW}$  is nearly parallel to the angular momentum contours.

in the boundary layer, while the  $R_{MW}$  slopes outward. The thick lines in Figs. 2a and 2b show the modifications to the angular momentum and azimuthal velocity due to friction. In most of the boundary layer, the wind is reduced by friction and the angular momentum surfaces have a significant outward displacement with decreasing elevation. Near the surface, the  $R_{MW}$  thus has markedly lower  $M$  than above the boundary layer, consistent with the opposite slopes of the  $R_{MW}$  and the  $M$  surfaces. A slight exception to this situation occurs near the top of the boundary layer, where a layer of supergradient flow (gray shading in Fig. 2) is associated with a smaller inward displacement of the angular momentum surfaces, and a slight outward kink in the  $R_{MW}$  that is likely undetectable in practice.

The method frequently used to estimate  $V_{mss}$  from flight-level data is the “90% rule” (Franklin et al. 2003) based on comparing flight-level winds near the eyewall with surface winds measured by GPS sondes (Hock and Franklin 1999). A limitation of the Franklin et al. (2003) study is that their reduction factor ( $F_r$ ) appears to be based on the measurement at the time the sonde is launched, rather than the maximum flight-level wind for the radial leg ( $V_{mxf}$ ). Sondes are typically launched radially inward from  $R_{mxf}$  in an attempt to sample  $V_{mss}$  (OFCM 2007), that is, in the zone of large  $F_r$  gradient.

To illustrate the difficulty of estimating the  $F_r$  from the GPS sondes, a set of 742 eyewall GPS sondes (and the maximum flight-level wind associated with their radial launch leg) was assembled for 17 hurricanes from 1997 to 2003. Pairs of 10-m wind speed and  $V_{mxf}$  were selected by wind speed ( $V_{mxf} > 33 \text{ m s}^{-1}$ , 10-m sonde wind  $> 30 \text{ m s}^{-1}$ ), flight altitude (2–4 km), and ratio of the radius of sonde 10-m wind to  $R_{mxf}$  (between 0.5 and 1.5). The selection process resulted in a set of 147 data pairs with a mean ratio (standard deviation; see Fig. 3) of the sonde 10-m level wind to  $V_{mxf}$  of 0.81 (0.14). For the 62 sondes launched near the 700-mb level, the  $F_r$  values [i.e., using flight-level wind at the time of sonde launch ( $V_f$ ) for the denominator] were 0.89 (0.18), which are nearly identical to the values of Franklin et al. (2003). Therefore,  $F_r$  based on the  $V_f$  will be larger than a ratio based on the  $V_{mxf}$  unless the sonde is launched at  $R_{mxf}$ . On the other hand, a sonde launched at  $R_{mxf}$  will typically reach the surface outside the  $R_{mss}$ , so that it would be unlikely such a sonde would detect the  $V_{mss}$ . Thus, a reduction factor for estimating  $V_{mss}$  is very difficult to determine from GPS sondes; the best estimate would come from using the highest surface value along a radial flight leg from multiple sondes launched inside of  $R_{mxf}$ .

For this study, the slant-maximum reduction factor ( $F_{rmx}$ ) is defined based on the ratio of  $V_{mss}$  to  $V_{mxf}$  for a given radial flight leg; that is, we calculate the reduction factor along the sloping  $R_{MW}$ , rather than near vertically from GPS sondes as in Franklin et al. (2003). It will be demonstrated that this approach explains more of the variance than do previous methods. When surface wind measurements are not available,  $F_{rmx}$  may be used to estimate  $V_{mss}$  from the maximum reconnaissance flight-level wind speed. This new  $F_{rmx}$  is also expected to be highly useful for retrospective studies of historical storms for which only reconnaissance flight-level data were available prior to the introduction of the GPS sonde and the Stepped Frequency Microwave Radiometer (SFMR; Uhlhorn and Black 2003).

The SFMR, which samples surface wind speed at high radial resolution, has been extensively compared to and

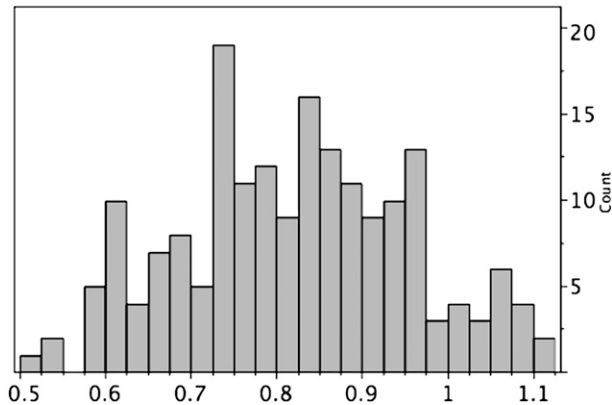


FIG. 3. Histogram of the ratio of 10-m GPS sonde wind speed to maximum flight-level wind speed from 147 sondes launched in the vicinity of the eyewall from 1997 to 2003. Mean ratio is 0.81, and the std dev is 0.14.

calibrated against GPS sondes (Uhlhorn et al. 2007). Since both  $V_{\text{mxs}}$  and  $V_{\text{mx f}}$  are sampled, the surface wind factor along the sloping  $R_{\text{MW}}$  ( $F_{\text{rmx}}$ ) may be reliably and easily computed for the first time. This paper discusses  $F_{\text{rmx}}$  based on SFMR and flight-level wind speed measurements. Section 2 will discuss the data and methods, results will be presented in section 3, discussion in section 4, and then conclusions in section 5.

## 2. Methods

### a. Aircraft in situ data systems and sampling strategies

The location information and winds measured at flight level are determined from data collected by the aircraft inertial and GPS navigation system and have an accuracy of  $0.4 \text{ m s}^{-1}$  for wind and 100 m for position based on aircraft intercomparison and calibration flights (Khelif et al. 1999). The aircraft flight patterns are designed to fulfill specific experiment goals and, typically, represent “figure 4” or “butterfly” patterns with several radial flight legs over an 8–10-h mission. Radial legs typically extend 100–200 km from the center. Additional information on specific National Oceanic and Atmospheric Administration (NOAA) Hurricane Research Division (HRD) Hurricane Field Program (HFP) flights and experiments can be found on the HFP Web site (information online at [www.aoml.noaa.gov/hrd](http://www.aoml.noaa.gov/hrd)) and in recent papers describing the 2005 Intensity Forecasting (IFEX) and the Rainband (RAINEX) Experiments (Rogers et al. 2006; Houze et al. 2006).

### b. SFMR data

A rigorous calibration–validation program of the SFMR instrument carried out during 2004 and 2005 HFP

involved engineers and scientists 1) monitoring the instrument while flying aboard the NOAA P3 aircraft, 2) evaluating the measurements transmitted in real time to the National Hurricane Center using the HRD Hurricane Wind Analysis System (H\*Wind), 3) interacting with forecasters to interpret the observations, and 4) sequentially improving the instrument calibration and geophysical emissivity–wind speed model based on comparisons with nearby GPS dropsonde measurements (Uhlhorn et al. 2007).

The revised wind speed–emissivity relationship was used to reprocess SFMR winds for hurricane datasets measured by the HRD SFMR (purchased in 1996), which includes hurricanes from 1998 to 2004. For 2005, the NOAA Aircraft Operations Center (AOC) installed the AOC SFMR aboard the NOAA P3 43RF. The AOC SFMR has better signal to noise ratios in the received signal but is otherwise similar to the earlier instrument, and was also reprocessed with the revised wind speed–emissivity relationship.

In this study, only data at flight levels 2–4 km are considered, which results in 179 radial legs from 35 missions into 15 hurricanes (Table 2). The SFMR and flight-level measurements recorded at a nominal rate of 1 Hz were filtered with a 10-s-centered running-mean filter. Each radial flight leg was examined to select the maximum flight-level wind speed  $V_{\text{mx f}}$  and the maximum SFMR surface wind  $V_{\text{mxs}}$ . All positions of maxima were located in terms of scaled (by  $R_{\text{mx f}}$ ) radial coordinates and storm-relative azimuth ( $A_z$ , measured clockwise from the storm heading). Detailed storm tracks were developed from spline fits of the vortex center fixes [derived by the method of Willoughby and Chelmon (1982)] from each flight. Flight legs over coastal or island locations were not included.

Since the SFMR responds to emissivity from wave breaking, and wind–wave interactions vary azimuthally around the storm as shown by Wright et al. (2001) and Walsh et al. (2002), it is important to evaluate the SFMR against collocated GPS sondes. The SFMR–GPS sonde wind speed difference as a function of azimuth by Uhlhorn and Black (2003, Fig. 9) was updated (Fig. 4) based on data reprocessed with the new geophysical model function for computing SFMR surface wind speeds from emissivity. The 416 GPS dropsonde–SFMR pairs consisted of SFMR observations at the time of the GPS sonde launches, and the GPS sonde surface wind estimated from the mean of the lowest 150 m of wind measurements (WL150; Franklin et al. 2003). In extreme winds, insufficient satellite signals sometimes cause the wind calculation to fail at low levels. Therefore, WL150-estimated surface winds were excluded if the lowest altitude for a measured wind from the sonde exceeded

TABLE 2. List of storms and flights in which SFMR data were collected.

Storm	Flight ID No.	No. of radial legs	Storm speed (m s <sup>-1</sup> )
Bonnie	19980826I	8	3.8
Earl	19980902I	1	8.4
Bret	19990822I	6	6
Floyd	19990913I	8	4
Floyd	19990915I	5	13
Lenny	19991116I	4	9.5
Humberto	20010923I	1	5.1
Lili	20020930I	1	5.1
Fabian	20030902I	8	4.2
Isabel	20030912I	6	4.9
Isabel	20030913I	4	5.3
Isabel	20030914I	2	6.1
Frances	20040830I	6	7.1
Frances	20040831I	4	7.5
Frances	20040901I	6	5.1
Frances	20040902I	2	10.7
Frances	20040903I	2	3.3
Frances	20040904I	3	2.4
Ivan	20040907I	8	7.7
Ivan	20040909I	6	5.8
Ivan	20040912I	4	4.6
Ivan	20040913I	3	4
Ivan	20040914I	12	4.6
Ivan	20040915I	10	4.2
Jeanne	20040925I	8	5
Katrina	20050827I	7	2.9
Katrina	20050828I	10	6.6
Katrina	20050829I	4	6.8
Ophelia	20050909I	1	4.5
Ophelia	20050911I	3	2.4
Rita	20050919I	1	5.6
Rita	20050920I	6	7
Rita	20050921I	8	7.3
Rita	20050922I	10	4.6
Rita	20050923I	8	6.7

150 m. Differences were bin averaged in 30° sectors and fit as shown in Fig. 4 together with the number of samples and the standard deviation of the differences in each bin. A harmonic fit to the differences results in

$$\text{SFMR} - \text{GPS} = 2.02 \cos(A_z + 27). \quad (1)$$

We apply Eq. (1) to correct the SFMR wind measurements for nonwind sources of roughness related to storm regions where windsea wave breaking is influenced by swell. In the right-rear quadrant of the storm, the swell and wind are propagating (moving) in the same direction, which causes the swell to grow and leave less foam (fewer breaking waves), hence resulting in negative differences. In the left-front quadrant, the swells may propagate against or across the wind, which leads to more breaking and more foam generation than wind seas alone (positive differences).

### 3. Statistical results and physical interpretation

Radial leg wind maxima pairs were analyzed to understand the dependence of  $F_{\text{rmx}}$  on storm characteristics that may be computed from flight-level quantities and other storm information. In particular, we establish an observational and theoretical basis for the location of the surface maximum wind relative to the maximum at flight level, and the relationship of  $F_{\text{rmx}}$  to  $R_{\text{mxf}}$ , eyewall slope, flight-level angular momentum, inertial stability, storm-relative azimuth, and storm motion. To gain further insight into the relationship between maximum surface and flight-level winds, observed characteristics are then compared to simulations from the Kepert and Wang (2001) tropical cyclone boundary layer model. An  $F_{\text{rmx}}$  model is developed through screening regression, and evaluated against other methods that have been used to estimate surface winds from flight-level wind measurements. Finally, we will revisit significant Atlantic basin hurricanes to provide updated estimates of intensity.

#### a. Distribution of $F_{\text{rmx}}$ and $R_{\text{mxs}}$

When examining all 179 radial legs in our dataset, the mean  $F_{\text{rmx}}$  is 0.8346 with a standard deviation of 0.09. Considerable variability exists about the mean  $F_{\text{rmx}}$  in Fig. 5 but the scatter is much less than that for  $F_r$  (0.19) reported by Franklin et al. (2003). The low  $F_{\text{rmx}}$  outliers of 0.5 and 0.6 are both from Hurricane Ophelia on 11 September of 2005. Ophelia was characterized by a relatively flat radial profile of flight-level wind speed, so the large (>80 km) values of  $R_{\text{mxf}}$  were based on rather subtle maxima. The high  $F_{\text{rmx}}$  values > 1.05 are from two legs in Hurricane Ivan on 7 and 9 September 2005, and one leg in Hurricane Frances on 31 August 2004, and are associated with small (<30 km) values of  $R_{\text{mxf}}$ . Franklin et al. (2003) have associated low and high values of  $F_r$  with stratiform and enhanced convective activities, respectively. However, Kepert (2001) and Kepert and Wang (2001) have shown that  $F_r$  may vary spatially in idealized boundary layer models that do not contain representations of convective processes. Rather, the hurricane boundary layer dynamics are such that horizontal advection of angular momentum<sup>2</sup> plays an important role in determining the wind structure. In particular, the eyewall is associated with a marked radial gradient of angular momentum that, coupled with

<sup>2</sup> The angular momentum advection is much more important at the surface because the inflow is much stronger there. In the boundary layer, the azimuthal wind budget is close to a balance between radial advection of angular momentum and frictional destruction. The advection peaks near the eyewall, where both the gradient and the inflow are large, hence giving a large  $F_r$ .



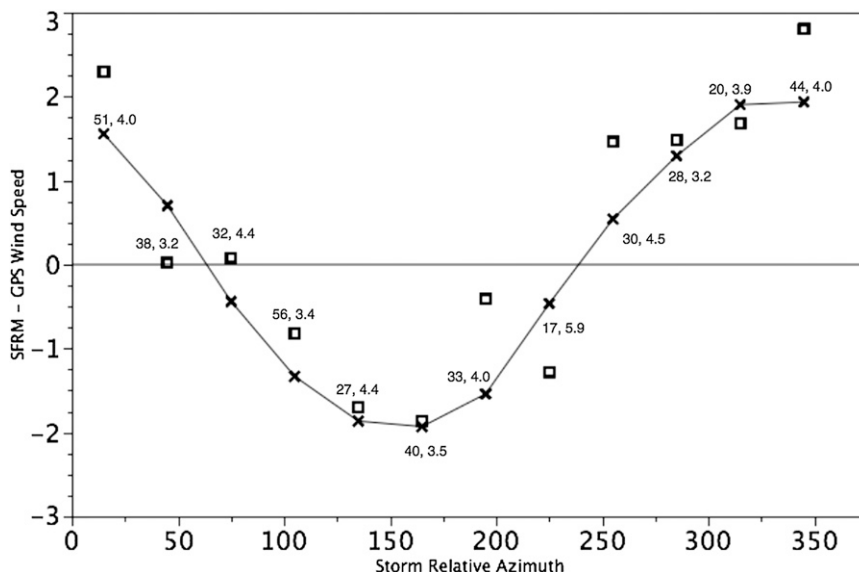


FIG. 4. Storm-relative azimuthal variation of bin-averaged SFMR-GPS sonde wind speed differences ( $\text{m s}^{-1}$ ). Curve with x's represents a harmonic fit to the bin-averaged differences (squares) and the azimuth is measured clockwise from the direction of storm motion. Numbers refer to bin sample size, and the std dev of the bin wind speed differences.

the frictionally forced inflow, can produce supergradient winds in the upper boundary layer and maintain relatively strong winds near the surface. This process explains the observed high  $F_r$  without the need to invoke additional processes (e.g., convective transport). Similar processes would be expected to operate near outer wind maxima, but probably to a lesser degree. Kepert (2006a,b) analyzed the boundary layer flow in the intense Hurricanes Georges and Mitch of 1998 and found strong quantitative and qualitative agreement with the model results for these storms through the depth of the boundary layer. The boundary layer dynamics associated with wind maxima also generate a frictionally forced updraft (Eliassen 1971; Kepert 2001; Kepert and Wang 2001). Thus, it appears that the physical cause for the statistical relationship between high values of  $F_r$  and strong vertical motion found by Franklin et al. (2003) may be that both are associated with the local wind maximum, rather than that the high  $F_r$  values are caused by the convective vertical motion.

Values of  $F_{\text{rmax}}$  were found to be negatively correlated (Fig. 6) with  $R_{\text{mxf}}$  and also to be higher on the left side of the storm than on the right. Kepert (2001) developed a linear analytical model of the tropical cyclone boundary layer, from which he derives a nonlinear analytical expression for the surface wind reduction factor  $F_r$ :

$$F_r = \frac{(\chi^2 + 2\chi + 2)}{(2\chi^2 + 3\chi + 2)}, \tag{2}$$

where

$$\chi = C_D V_g \sqrt{\frac{2}{KI}}, \tag{3}$$

where  $C_D$  is the drag coefficient,  $V_g$  is the gradient wind,  $K$  is the boundary layer mean vertical diffusivity, and  $I$  is the inertial stability. Other things being equal, the inertial stability at the  $R_{\text{MW}}$  will be higher for a smaller  $R_{\text{MW}}$ , so (2) predicts that  $F_{\text{rmax}}$  will be larger for a smaller

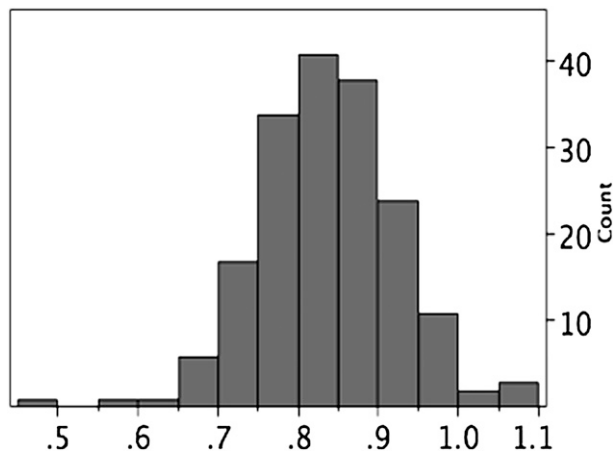


FIG. 5. Distribution of slant reduction factor  $F_{\text{rmax}}$  determined from SFMR-measured surface wind maxima and flight-level wind maxima from 179 radial legs in 15 hurricanes. Mean is 0.83, and std dev is 0.09.

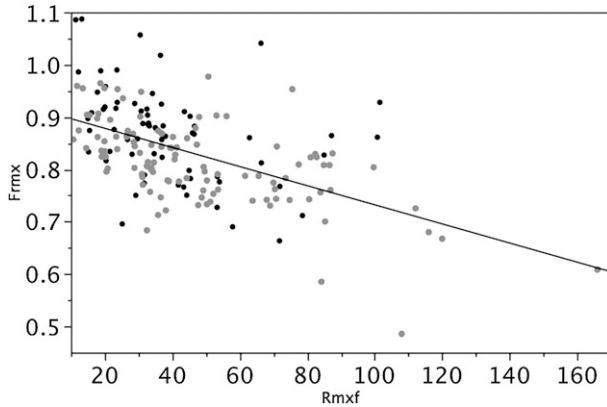


FIG. 6. Corresponding values of slant reduction factor  $F_{\text{rmx}}$  and  $R_{\text{mxf}}$ , where black (gray) points represent locations on the left (right) side of the storm. The least squares fit line explains 28% of the variance.

$R_{\text{MW}}$ , consistent with the negative correlation shown in Fig. 6. The left–right asymmetry in  $F_{\text{rmx}}$  found here was first predicted by Kepert (2001) and Kepert and Wang (2001), and subsequently found in Franklin et al.’s (2003) observational analysis. Case studies of individual storms by Kepert (2006a) and Schwendike and Kepert (2008) have also shown the presence of this asymmetry.

The majority of surface wind maxima are found radially inward from the flight-level wind maximum. The mean value of  $R_{\text{mxs}}/R_{\text{mxf}}$  is 0.875 (Fig. 7) with a standard deviation of 0.16. No consistent azimuthal variation of  $R_{\text{mxs}}/R_{\text{mxf}}$  was apparent, possibly because environmental shear can tilt the storm axis in any direction relative to the motion, and this effect dominates any motion-induced asymmetry in this parameter. The  $R_{\text{mxs}}/R_{\text{mxf}}$  outliers  $> 1.5$  are associated with storms undergoing concentric eyewall cycles (Willoughby et al. 1982) in which the surface wind in the newly forming outer eyewall exceeds the maximum flight-level wind in the decaying inner eyewall (e.g., Ivan on 15 September 2005). Outliers  $< 0.5$  represent cases in which the  $V_{\text{mxs}}$  is still found in the inner eyewall but the  $V_{\text{mxf}}$  is located in the outer eyewall (two other flight legs in Ivan on 15 September and two legs in Jeanne on 25 September 2005). The  $R_{\text{mxs}}/R_{\text{mxf}}$  outliers were not associated with outlying values of  $F_{\text{rmx}}$ .

#### b. $F_{\text{rmx}}$ , angular momentum, and eyewall slope

Angular momentum  $M$ , or a function thereof, is a physically appealing choice for an independent variable in a regression for  $F_{\text{rmx}}$  because  $M$  is nearly constant along the  $R_{\text{MW}}$  above the boundary layer, as discussed in the introduction and shown in Fig. 2. We now develop a simple approximation for  $F_{\text{rmx}}$  in terms of  $M$ . Two linear approximations to (2) valid at the  $R_{\text{MW}}$ , which we

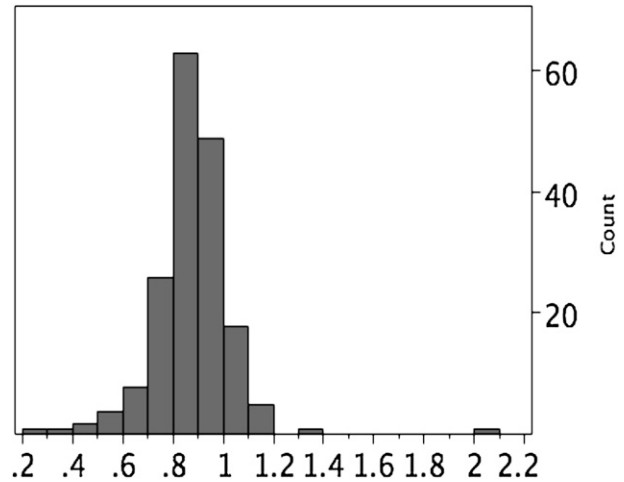


FIG. 7. As in Fig. 5 but for distribution of  $R_{\text{mxs}}/R_{\text{mxf}}$ .

will use to guide our choice of dependent variables in subsequent statistical regressions, are

$$F_r \approx 0.95 - 9.2 \times 10^{-5} \sqrt{M} \quad (4)$$

and

$$F_r \approx 0.88 - 3.3 \times 10^{-8} M. \quad (5)$$

The derivations of (4) and (5) are given in the appendix. Comparison of (4) and (5) with (2) showed that (4) was somewhat more accurate (not shown), but both are quite reasonable, so we seek a statistical linear relationship between  $F_{\text{rmx}}$  and either angular momentum or its square root at  $R_{\text{MW}}$ .

Relative angular momentum per unit mass was computed at  $R_{\text{mxf}}$  assuming that the flight-level radial wind component is small. Here,  $F_{\text{rmx}}$  is negatively correlated with flight-level relative angular momentum and its square root (Fig. 8). The lines of best fit to  $M$  are

$$F_{\text{rmx}} = 0.93 - 3.89 \times 10^{-8} M \quad \text{and} \quad (6)$$

$$F_{\text{rmx}} = 1.028 - 1.27 \times 10^{-4} \sqrt{M}, \quad (7)$$

which are in good agreement with the analytical approximations (4) and (5), and explain 31% and 32% of the variance, respectively. The close agreement between (4) and (7) and (5) and (6) provides evidence of the validity of Kepert’s (2001) linear model.

We now consider the relationship between flight-level and surface angular momentum at the respective wind maxima. Unfortunately, the SFMR instrument does not measure surface wind direction, but the surface tangential velocity component is estimated by assuming a constant inflow angle of  $23^\circ$ , based on examination of

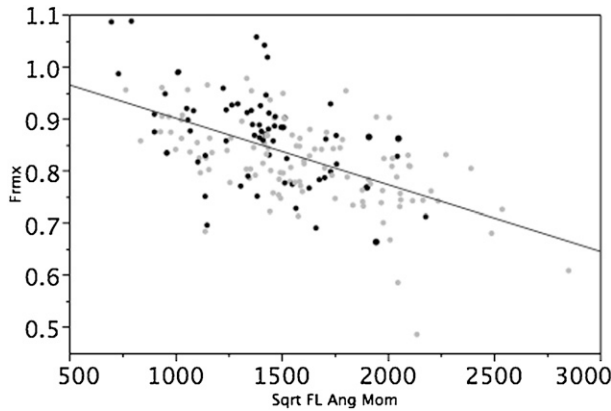


FIG. 8. Slant reduction factor  $F_{rmx}$  vs the square root of the flight-level relative angular momentum per unit mass ( $m^2 s^{-1}$ ) at the  $R_{MW}$ , where the black (gray) points represent the left (right) side of the storm. Linear least squares fit line explains 32% of the variance.

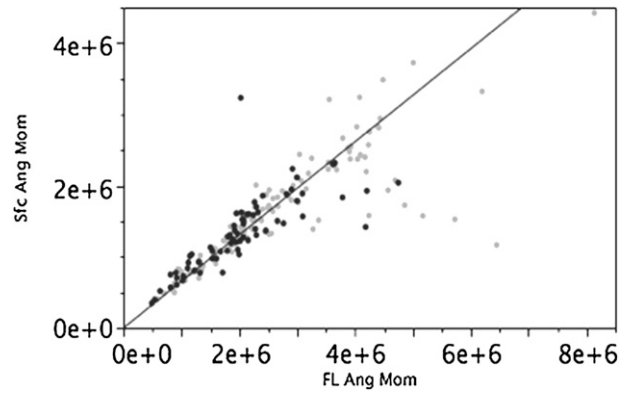


FIG. 9. Surface vs flight-level relative angular momentum per unit mass ( $m^2 s^{-1}$ ) where black (gray) points represent the left (right) side of the storm. Line represents the eyeball fit constrained to the origin.

near-surface inflow angles from 881 GPS sonde profiles. Comparing surface relative angular momentum at  $R_{mxs}$  with flight-level angular momentum at  $R_{mxf}$  (Fig. 9) indicates that momentum is not constant along a line connecting the two wind maxima, consistent with Fig. 2 and the discussion in the introduction. A linear fit constrained to pass through the origin of Fig. 9 shows that the surface relative angular momentum at  $R_{mxs}$  is about 65% of the flight-level relative angular momentum at  $R_{mxf}$ . Mean values of  $V_{mxs}$ ,  $R_{mxs}$  and  $V_{mxf}$ ,  $R_{mxf}$  yield a slightly higher angular momentum reduction factor of  $\sim 75\%$ . These fractions are associated with the loss of relative angular momentum due to surface friction, although correct interpretation requires some care as several processes are operating. The surface  $R_{MW}$  has a significantly lower value of  $M$  than the  $R_{MW}$  above the boundary layer because it has lighter winds and is at smaller radius. Comparing the angular momentum reduction factor of 0.65–0.75 found here with the mean  $F_{rmx}$  of 0.83 suggests that the surface  $R_{MW}$  is  $\sim 80\%$ – $90\%$  of that at flight level (the observed mean  $R_{mxs}$  is about 90% of  $R_{mxf}$ ). These arguments are consistent with conceptual models of angular momentum surfaces in hurricanes (Emanuel 1986; Kepert and Wang 2001; see also Fig. 2 above), with increases of  $R_{MW}$  with height from the surface to the top of the boundary layer, followed by a further outward tilt of both the  $R_{MW}$  and the angular momentum surfaces with height above the boundary layer, and a concomitant decrease in angular momentum with height (Fig. 2).

Given the above estimate of the frictional loss of relative angular momentum,

$$V_{mxs}R_{mxs} = 0.65V_{mxf}R_{mxf}, \quad (8)$$

then

$$F_{rmx} = 0.65R_{mxf}/R_{mxs}. \quad (9)$$

Hence,  $F_{rmx}$  should also depend on the slope of the eyewall wind maxima, with smaller values for near-vertical wind maxima and larger values for eyewalls with wind maxima that tilt farther outward with height. This is physically consistent with the idea that  $M$  is close to constant along the  $R_{MW}$  above the boundary layer. Therefore, the near-vertical case will have nearly constant wind speed along the  $R_{MW}$  above the boundary layer, while the strongly tilted case will have much stronger winds immediately above the boundary layer than farther aloft. However, the  $F_{rmx}$  observations show little dependence on relative  $R_{MW}$  slope (Fig. 10) due to the variety of storm eyewall diameters. If a wind maximum slopes greatly outward in a large-diameter eyewall, the inverse dependence of  $F_{rmx}$  on  $M$  [Eq. (6)] contributes to smaller  $F_{rmx}$  while the large outward tilt contributes to a larger  $F_{rmx}$  [Eq. (9)]. However, all values of  $F_{rmx} > 1.0$  in Fig. 10 also have relatively large values of relative  $R_{MW}$  slope. The largest slopes in Fig. 10 are related to outer flight-level wind maxima associated with concentric eyewall processes mentioned earlier.

*c.  $F_{rmx}$  and inertial stability*

Modeling by Kepert and Wang (2001) suggests that a strong radial gradient of angular momentum together with high values of inertial stability helps force the eyewall updraft to be located at the radius of maximum wind. Vertical advection of the inflow and radial advection of the angular momentum act to generate a low-level jet at the  $R_{MW}$  near the top of the boundary layer. Investigations of GPS sonde data (Franklin et al. 2003; Powell et al. 2003) show the jet level is near 400–500 m, in



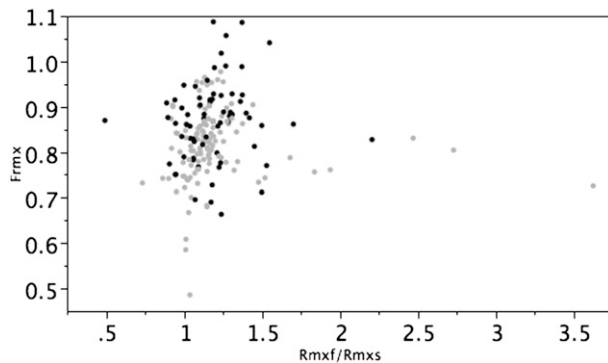


FIG. 10. Slant reduction factor  $F_{rmx}$  vs relative slope of the wind maximum. Black (gray) points represent the left (right) side of the storm.

agreement with this work. Recent comparisons by Kepert (2006a,b) shows that the Kepert and Wang tropical cyclone boundary layer model is capable of reproducing many of the features observed in GPS sonde profiles.

Inertial stability is computed at  $R_{mxf}$  by assuming a zero radial gradient of tangential velocity at flight level, and ignoring the Coriolis term, which results in  $I \approx \sqrt{2} V_{mxf}/R_{mxf}$ . The slant reduction tends to increase with inertial stability (Fig. 11 with a 22%  $r^2$  for the linear fit), and higher values on the left side of the storm than on the right.

#### d. Azimuthal variation of $F_{rmx}$

Thus far, we have seen that the slant reduction factor is largest with small  $R_{mxf}$ , which also correlates with small relative angular momentum and large inertial stability. In addition, larger  $F_r$  values are found on the left side of the storm than the right, in agreement with the findings of Franklin et al. (2003) and Kepert (2006a,b). Franklin et al. (2003) commented that  $F_r$  was 4% higher on the left side than the right side of the storm. This overall pattern of lower  $F_r$  values on the stronger wind side of the storm and higher  $F_r$  values on the weaker is also consistent with the predictions of Kepert (2001) and Kepert and Wang (2001).

Front-to-back and left-to-right transects of the 10-m (thick line) and surface gradient (thin line) winds are shown in Fig. 12 for an intense tropical cyclone moving at various speeds according to the model of Kepert and Wang (2001). Forcing to the model was provided by a parametric profile according to Willoughby et al. (2006), with a maximum symmetric gradient wind speed of  $60 \text{ m s}^{-1}$  at a radius of 25 km, divided between exponential length scales of 65 and 500 km in the ratio 35:25, a blending width of 15 km, and an inner shape exponent of 0.9. In this figure, the 10-m wind is taken directly from the model and the surface gradient wind is from the

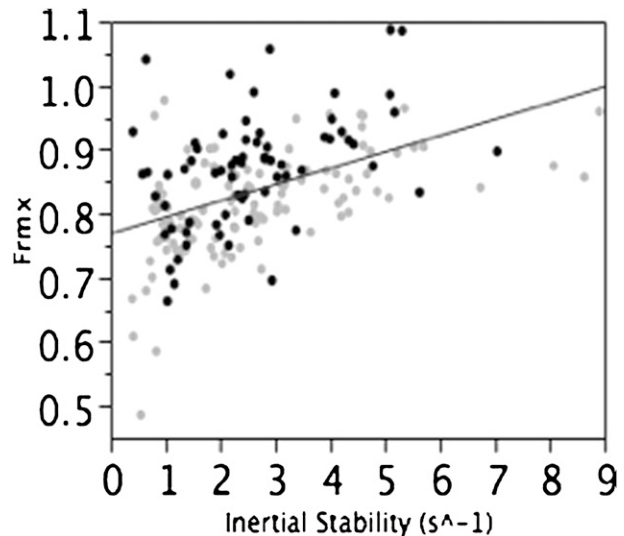


FIG. 11. Slant reduction factor  $F_{rmx}$  vs flight-level inertial stability ( $s^{-1}$ ) computed from  $I \approx 1.414 V_{mxf}/R_{mxf}$ , where black (gray) points represent the left (right) side of the storm. Linear least squares fit line explains 22% of the variance.

parametric pressure profile used to force the model. The model does not include a warm core, but we approximately account for this effect by applying an assumed slope of the angular momentum surfaces with height to the surface gradient wind, to estimate the gradient wind at 3-km height (dashed lines). The assumed slope of the  $M$  surfaces is taken to be proportional to the radius, with a value of two at the surface radius of the maximum gradient wind. We emphasize that this is a somewhat arbitrary parameterization of the effect of the warm core on the surface wind reduction problem, although the assumed slope of the angular momentum surfaces is consistent with observations in intense hurricanes (e.g., Montgomery et al. 2006). The surface winds in Fig. 12 are a larger fraction of the gradient wind to the left than the right, with a smaller but still significant difference being applied front to back. This statement applies to both the surface gradient wind and that at 3 km. Moreover, the left-right transects for the modeled moving storm are strikingly similar to the transect shown from Hurricane Katrina (Fig. 1). Similarly, Shapiro (1983, his Fig. 5) found that the boundary layer mean wind speed was slightly higher in an absolute sense, and therefore a significantly greater fraction of the gradient wind, on the left of the storm than on the right.

Observations of  $F_{rmx}$  (Fig. 13) have a similar sinusoidal variation with lower mean values (0.79) in the front through the right side of the storm from azimuth ( $A_z$ ) 330 through azimuth 130, and higher mean values (to 0.89) mainly in the left-rear and left-front azimuths

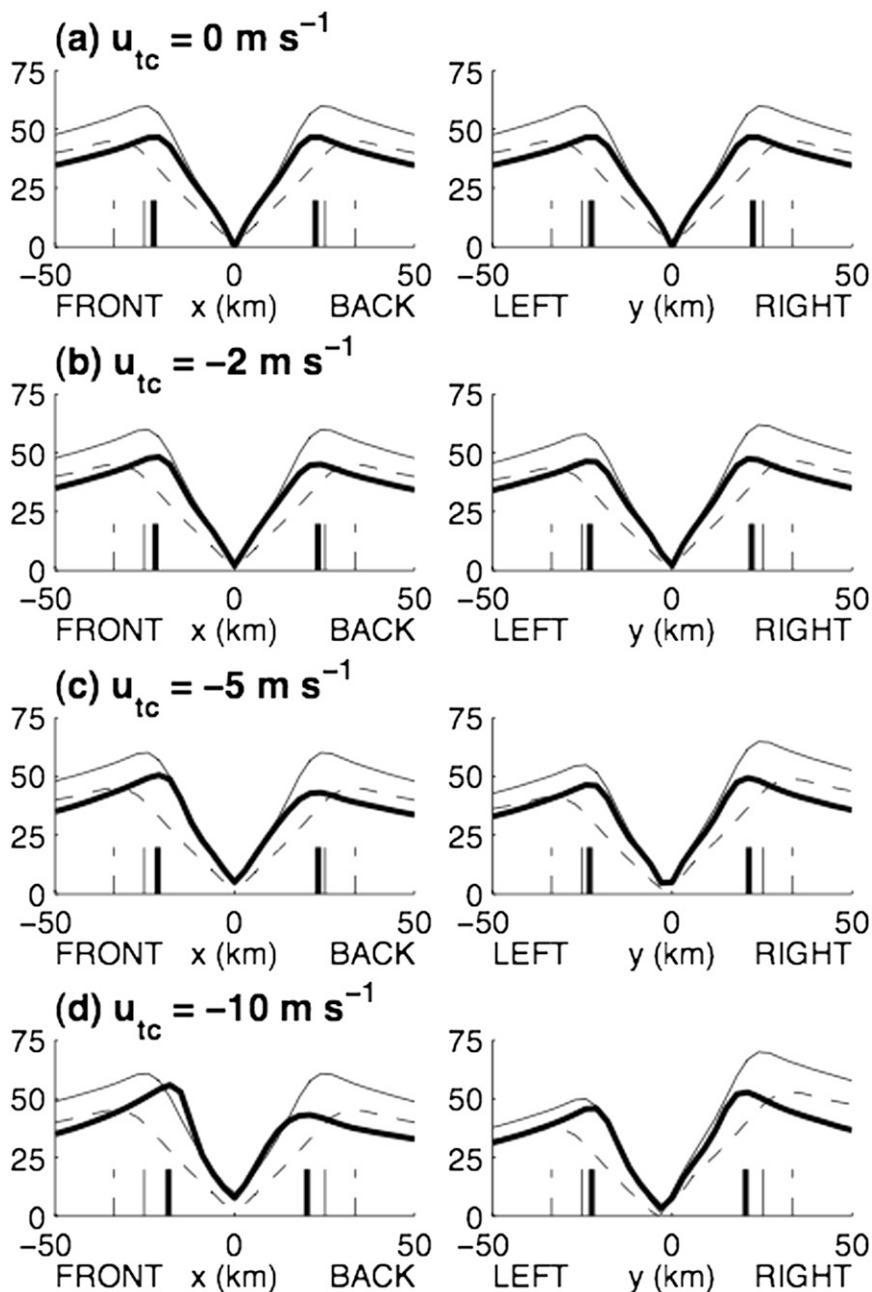


FIG. 12. Transects of 10-m (thick line), surface gradient (computed from surface pressure, thin line), and 3-km level gradient (green line) wind speeds in a hurricane simulated using the model of Kepert and Wang (2001). Storm translation speeds are (a) 0, (b) 2, (c) 5, and (d) 10  $\text{m s}^{-1}$ . The short vertical lines on the abscissa indicate the radius of maximum winds at the respective levels.

170–310. An azimuthal fit that explains 15% of the variance is shown in Fig. 13:

$$F_{\text{rmx}} = (0.841 - 0.050) \sin(A_z + 38). \quad (10)$$

Clearly, the azimuthal variation will be an important quantity for developing a model to diagnose the slant reduction factor from flight-level observations.

Kepert and Wang (2001) found that the boundary layer maximum wind jet became increasingly more pronounced on the left side of the storm as the storm motion increased. Similarly, the 10-m and gradient winds are nearly coincident on the left side for fast-moving storms in Fig. 12. Hence, some of the variability in slant reduction factors may be related to storm motion.

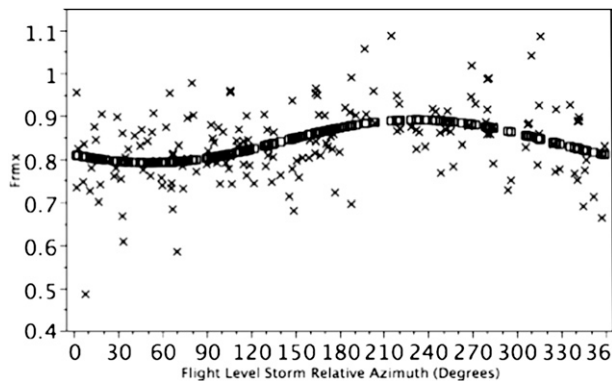


FIG. 13. Storm-relative azimuthal variation of slant reduction factor  $F_{\text{rmx}}$  (crosses) and sinusoidal fit [Eq. (10), squares].

Mean storm motion for each flight was evaluated from a spline fit to flight-level wind centers. While there is considerable scatter and only 6% of the variance is explained by a linear fit,  $F_{\text{rmx}}$  generally increases with storm motion (Fig. 14), with left-side  $F_{\text{rmx}}$  values remaining higher than those on the right.

#### e. Regression-based maximum surface wind estimation methods

Since a reconnaissance flight mission typically takes place over a 6-h forecast cycle, the maximum winds measured during a complete reconnaissance mission have a large influence on the intensity estimate. Three surface wind estimation techniques were developed, all using flight-level information as input. The first is designed to estimate the maximum surface winds for a particular radial flight leg. The second estimates the maximum surface wind based on the radial leg containing the maximum flight-level wind speed anywhere in the storm, and the third and final method estimates the maximum surface wind speed anywhere in the storm, regardless of the location of the radial leg.

##### 1) ESTIMATING THE MAXIMUM SURFACE WIND ON A RADIAL FLIGHT LEG

A variety of candidate predictors were evaluated in a stepwise screening regression using JMP statistical software (version 7; information online at <http://www.jmp.com/>). The screening process led to a multiple linear least squares regression that explains 41% of the variance:

$$F_{\text{rmx}} = 0.825 - 2.41 \times 10^{-8}M + 8.64I + (0.009C_t - 0.0332) \sin(A_z + 38), \quad (11)$$

where  $C_t$  is the storm translation speed in meters per second;  $M$  and  $I$  are the flight-level values at  $R_{\text{mx}}$ , respectively; and the azimuthal dependence term is from

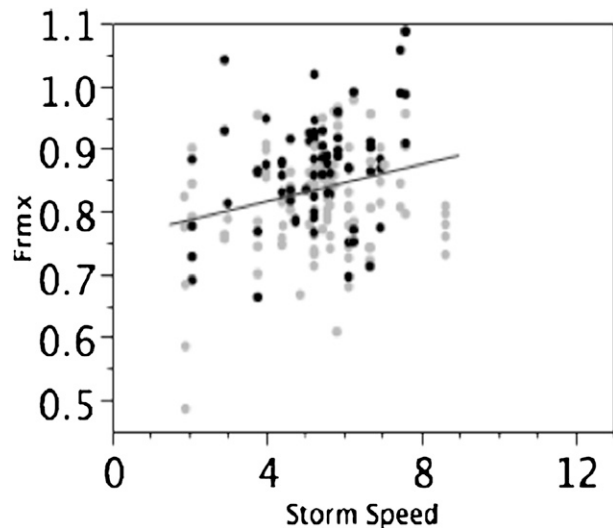


FIG. 14. Slant reduction factor  $F_{\text{rmx}}$  as a function of storm speed ( $\text{m s}^{-1}$ ).

Eq. (10). An important property of (11) is that it contains no reference to the flight-level altitude, which occurs because the term in (11) that explains most of the variance is the angular momentum term (the  $\sqrt{M}$  term was of nearly the same importance). As previously discussed, the angular momentum above the boundary layer is nearly constant along the sloping  $R_{\text{MW}}$ , while the wind speed variation through the boundary layer depends on the amount of slope and the distance from the flight level to the boundary layer top. Hence, the vertical variation of  $F_r$  with height specified by Franklin et al. (2003) is not needed in this formulation. Equation (11) is appropriate for estimating the maximum surface wind on each of several radial legs during a reconnaissance mission and is used in the HRD's real-time H\*Wind system (Powell et al. 1998; Powell and Houston 1996).

An evaluation of Eq. (11) with the observed maximum SFMR surface wind speeds using the developmental dataset results in a near-zero bias and an RMS error of  $3.6 \text{ m s}^{-1}$ , or 8% of the mean  $V_{\text{mxs}}$  (Table 3). Using the mean  $F_{\text{rmx}}$  value of 0.8346 results in a near-zero mean error and an RMS error of  $4.7 \text{ m s}^{-1}$ , so the regression (11) substantially improves the estimation accuracy.

Estimates of the error of earlier methods can be made by assuming the SFMR maximum values as "ground truth." Such error estimates for the mean 90% rule (Franklin et al. 2003), the eyewall tilt method of Dunion et al. (2003), and the 80% rule (Powell 1980) are shown in Table 3. Applying the 90% rule to the maximum flight-level wind speed for the particular flight leg results in a high bias of  $3.7 \text{ m s}^{-1}$  and an RMS error of  $6.0 \text{ m s}^{-1}$ . Notice in Fig. 13 that the slant wind reduction factor

TABLE 3. Errors in estimating maximum surface wind speeds from flight-level measurements between 2 and 4 km based on SFMR  $V_{\text{mxs}}$  measurements from 179 radial flight legs.

Reduction model	Bias ( $\text{m s}^{-1}$ )	RMS error ( $\text{m s}^{-1}$ )
SFMR based [Eq. (11)]*	0.001	3.62
0.8 at $R_{\text{mxf}}$	-2.08	5.21
0.9 at $R_{\text{mxf}}$	3.73	5.99
Eyewall tilt at $R_{\text{mxf}}$	8.31	10.53
Mean $F_{\text{rmx}}$ ( $0.8346 V_{\text{mxf}}$ )	-0.07	4.72

\* SFMR based errors use the developmental dataset.

approaches 90% only in the left-rear quadrant. It could be argued that this is an unfair comparison since the Franklin et al. (2003) technique used GPS sonde data in which the measurements contained much smaller radial displacements between sonde launch and splash radii, but larger tangential displacements than are being considered here between  $R_{\text{mxf}}$  and  $R_{\text{mxs}}$ . Thus, their eyewall  $F_r$  value tends to be higher than the  $F_{\text{rmx}}$  found here because their flight-level wind was measured somewhat inward of  $R_{\text{mxf}}$ . Regardless of this, operational practice (Franklin 2001) has evolved toward applying the 0.9 factor directly to the strongest measured flight-level wind, which will tend to bias the surface wind estimates high.

The eyewall tilt method of Dunion et al. (2003) was applied to the flight-level wind speed at  $R_{\text{mxf}}$  after first estimating a mean boundary layer wind using their Eq. (2) and then estimating the surface wind speed using their Eq. (5). The tilt method applied to the maximum flight-level wind speed at  $R_{\text{mxf}}$  is best suited to sharply peaked flight-level wind maxima and thus a high bias of  $8.3 \text{ m s}^{-1}$  and an RMS error of  $10.5 \text{ m s}^{-1}$  are found. The 80% rule of (Powell 1980) was also evaluated, and a bias of  $-2.1 \text{ m s}^{-1}$  and an RMS error  $5.2 \text{ m s}^{-1}$  were found. The 80% rule should be bias free only in the front-right quadrant of the storm (Fig. 13). The PBL models that assume the maximum flight-level winds are equivalent to mean boundary layer winds also underestimate surface winds when flight-level winds exceed  $55 \text{ m s}^{-1}$  (Powell et al. 1999).

### 2) ESTIMATING $V_{\text{Mxs}}$ BASED ON THE RADIAL LEG WITH THE LARGEST $V_{\text{Mxf}}$ FOR THE FLIGHT MISSION

A reduction factor over an entire reconnaissance mission ( $F_{\text{rmx1}}$ ) can be used to estimate the maximum surface wind associated with the radial flight leg containing the largest measured  $V_{\text{mxf}}$ . For this purpose, the largest  $V_{\text{mxf}}$  value (and the corresponding  $V_{\text{mxs}}$  on the same radial flight leg) is selected for each flight mission. Restricting the sample to 25 flights with three or more

radial legs with SFMR measurements,  $V_{\text{mxf}}$  was on the right side of the storm in all but one flight (Isabel 12I). A simplified expression for  $F_{\text{rmx1}}$ , depending only on  $V_{\text{mxf}}$  and inertial stability (I), explained more of the variance ( $r^2$  of 56%) than (11):

$$F_{\text{rmx1}} = 0.5887 + 0.0022V_{\text{mxf}} + 23.982I. \quad (12)$$

Equation (12) may be used to estimate the peak surface wind in the quadrant containing the peak flight-level wind over the course of a reconnaissance mission. The increase in variance explained by Eq. (12) relative to Eq. (11) implies that the surface maximum wind is more strongly related to the flight-level wind in the most intense quadrant of the storm than elsewhere.

Comparing the 90% rule to (12) (Table 4), the 90% rule is biased high by 11% with a 14% RMS error, while (12) has a small negative bias and a 4% RMS error (based on a mean  $V_{\text{mxs}}$  of  $53 \text{ m s}^{-1}$ ). The eyewall tilt method high bias is 8% with a 26% RMS error, and the 0.8 method has a low (2%) bias and 9% RMS error. Application of Eq. (12) is limited to estimating the maximum surface wind along the radial leg containing the maximum flight-level wind throughout the flight mission. However, for more than half of the 25 SFMR flight missions, the maximum surface wind anywhere in the storm was found on a different radial leg azimuth than that containing the maximum flight-level wind.

### 3) ESTIMATING MAXIMUM $V_{\text{Mxs}}$ ANYWHERE IN THE STORM

To estimate the highest  $V_{\text{mxs}}$  for the mission independent of the flight leg, the maximum  $V_{\text{mxf}}$  and  $V_{\text{mxs}}$  are selected for each mission and the sample is again restricted to missions with at least three radial legs. In all but four flights (Fabian 02I, Floyd 13I, Frances 31I, and Rita 21I),  $V_{\text{mxs}}$  was located on the right side of the storm. In 13 of these 25 flights,  $V_{\text{mxs}}$  was at a different azimuth than the  $V_{\text{mxf}}$ . On three missions (Fabian 02I, Floyd 13I, and Isabel 12I), significant azimuthal differences occurred with surface wind maxima on the opposite side of the storm from the flight-level maxima.

The maximum flight-level wind speed and radius are the most important predictors of the slant reduction factor ( $F_{\text{rmxa}}$ ) in determining the maximum surface wind anywhere in the storm over the course of a reconnaissance flight ( $r^2$  of 66%):

$$F_{\text{rmxa}} = 0.84123 + 0.001516V_{\text{mxf}} - 0.0026R_{\text{mxf}}. \quad (13)$$

Equation (13) is appropriate for retrospective evaluation of the maximum intensity over the course of a reconnaissance mission.



TABLE 4. Evaluation of  $V_{\text{mxs}}$  for the radial leg containing the largest  $V_{\text{mxf}}$  for the mission [Eq. (12)] based on 25 missions in 12 storms. Here,  $V_{\text{mxs}}$  is the SFMR measurement associated with the radial flight leg in which the maximum  $V_{\text{mxf}}$  is measured over the entire flight.

$V_{\text{mxs}}$ source	Bias ( $\text{m s}^{-1}$ )	RMS error ( $\text{m s}^{-1}$ )
SFMR based [Eq. (12)]	-1.2	2.2
0.8 at $R_{\text{mxf}}$	-0.2	4.6
0.9 at $R_{\text{mxf}}$	6.3	7.6
Eyewall tilt at $R_{\text{mxf}}$	4.8	15.1

The increase in variance explained by Eq. (13) relative to Eq. (12) is probably due to the fact that the azimuth of the maximum wind may vary with height in the storm due to asymmetric friction (Kepert 2001; Kepert and Wang 2001; Kepert 2006a,b; Schwendike 2005) and to environmental shear (e.g., Frank and Ritchie 2001; Jones 1995). Considering that the maximum flight-level and surface winds may appear in different quadrants in this regression, as they do in nature, thus reduces the amount of random scatter. The greater amount of variance explained in Eq. (13) is a most useful property, as the maximum surface wind, anywhere in the storm, is highly important parameter for operational forecasting and warning.

Estimation from Eq. (13) of the peak  $V_{\text{mxs}}$  of all radial legs within the storm is relevant to estimation of the maximum surface wind in a storm for operational and historical retrospective analysis applications. Based on the developmental data, Eq. (13) results in an RMS error of  $< 5\%$ . Evaluation of other methods (Table 5) suggests that the 90% rule has a high bias (RMS) of 9% (12%), while the eyewall tilt method bias (RMS) is 26% high (28%), and the 0.8 method is 4% low (10%). Also included in Table 5 is the official “best track” (BT) estimate of the maximum wind from the National Hurricane Center based on tropical cyclone reports available from the NHC Web site (information online at <http://www.nhc.noaa.gov/pastall.shtml>). The BT estimates are very similar to the 90% method and are the basis for the historical record in the Hurricane Database (HURDAT) file (Jarvinen et al. 1988). This analysis is only valid for flight-level reductions in which the aircraft is flying within the 2–4-km altitude range, which is the common altitude for mature hurricanes. In tropical storms and weaker hurricanes, reconnaissance flights are often conducted at altitudes  $< 1.5$  km, and surface wind reduction factors are closer to 80% (Franklin et al. 2003).

It is apparent from Fig. 15 that the 90% method, and by implication portions of the recent historical record, are biased high for  $V_{\text{mxf}} < 75 \text{ m s}^{-1}$ . Application of (13) to flight-level measurements in historical storms would provide an assessment of the impact of the bias on

TABLE 5. As in Table 4 but for the evaluation of the largest  $V_{\text{mxs}}$  measured anywhere in the storm.

Reduction model	Bias ( $\text{m s}^{-1}$ )	RMS error ( $\text{m s}^{-1}$ )
SFMR based [Eq. (13)]	0.0	2.5
0.8 at $R_{\text{mxf}}$	-1.9	5.2
0.9 at $R_{\text{mxf}}$	4.6	6.4
Eyewall tilt at $R_{\text{mxf}}$	14.1	15.1
Best track	4.3	6.3

the historical record, but the  $4.6 \text{ m s}^{-1}$  bias in the 90% method ( $\sim$  one-half a Saffir–Simpson scale category) suggests that hurricane activity is overestimated for categories weaker than a moderate category 4 hurricane, provided the reconnaissance aircraft were flying above 2 km. The transition of the SFMR to operational reconnaissance will make the 90% method obsolete for future operational estimates of surface winds in Atlantic hurricanes within aircraft range. The SFMR measurements and (13) can be used to help calibrate satellite hurricane intensity estimation methods (e.g., Olander and Velden 2007). The resulting updated satellite techniques could then be applied to improve intensity estimates for all tropical cyclone basins. These techniques may then be applied in reanalysis efforts to improve the historical record.

#### 4. Discussion

Equation (11) has been implemented in H\*Wind to estimate the maximum surface wind speed from an aircraft radial flight leg when reconnaissance measurements are available at the 2–4-km level. Installation of new SFMR units on the fleet of U.S. Air Force hurricane aircraft commenced in 2007 so future use of reduction factors will be limited to flights on which the instrument is not available. The  $F_{\text{mxf}}$  fit in Eq. (11) provides an improved estimate of the surface wind speed on a particular flight leg for cases in which the SFMR is not available. Equations (12) and (13) will be especially useful for improving estimates of the maximum surface wind from available flight-level observations in significant historical hurricanes. Additional studies are in progress to use Eqs. (12) and (13) to calibrate estimates of intensity from pattern recognition techniques applied to historical satellite imagery (C. Velden, S. Mullins, and P. Black 2007, personal communication). For cases in which the reconnaissance aircraft is flying below 2 km (typically tropical storms and weaker hurricanes), Dunion et al. (2003) found a strong correlation of flight-level wind speeds with mean boundary layer winds measured by GPS sondes. In those cases, the  $F_r$  values described in Franklin et al. (2003) may be adequate but await confirmation using SFMR data.



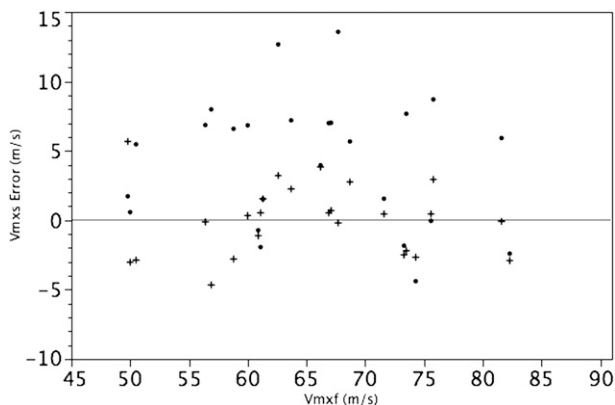


FIG. 15. The  $V_{mxs}$  error ( $m\ s^{-1}$ ) based on estimating the  $V_{mxs}$  ( $m\ s^{-1}$ ) from the maximum  $V_{mxf}$  for each flight mission containing at least three SFMR radial legs. Dots represent the 90% method and crosses are estimates from Eq. (13).

*a. Retrospective assessment of some significant Atlantic basin hurricanes*

Since the 90% method was used to revise the intensity of Hurricane Andrew (Landsea et al. 2004), a few cases are examined to illustrate how revised maximum surface wind estimates based on Eq. (13) and the 90% rule vary from those published in the National Hurricane Center’s HURDAT record.<sup>3</sup> Consistent with Fig. 15, the most intense storms have similar surface wind estimates from Eq. (13) and the 90% method (Table 6). However, application of Eq. (13) implies a low bias in the BT estimates of Hurricanes Allen, Gilbert, and Mitch.

*b. Evaluation of Eq. (11) from independent data collected during the 2006 Hurricane Field Program*

The SFMR-based regression Eq. (11) for the radial leg value of  $F_{rmx}$  was tested on an independent set of observations collected for two missions in Hurricane Helene on 17 and 19 September 2006, with a total of 10 radial flight legs available within the 2–4-km altitude range. These were the only SFMR data collected in a hurricane during the relatively inactive 2006 season and processed data for 2007 were not yet available at the time of this writing. The SFMR observations (Table 7) indicate a low bias of  $-0.7\ m\ s^{-1}$  for the Eq. (11) method and an RMS error of  $3\ m\ s^{-1}$  (or 8% based on the mean surface  $V_{mxs}$  of  $35.8\ m\ s^{-1}$ ). The 90% method has a  $4.5\ m\ s^{-1}$  high bias and a percentage RMS error of 15%. The other methods generally have similar error characteristics relative to each other (as shown in Table 3) but with smaller magnitudes.

TABLE 6. Estimates of  $V_{mxs}$  from Eq. (13) compared to the 90% rule and the BT for selected historical storms in which SFMR measurements were not available. With the exception of Andrew, which uses the peak 10-s flight-level wind speed,  $V_{mxf}$  values are from archived minob values.

Storm name and event time and date	$V_{mxf}$ ( $m\ s^{-1}$ )	$V_{mxs}$ Eq. (13) ( $m\ s^{-1}$ )	$V_{mxs}$ 90% ( $m\ s^{-1}$ )	BT ( $m\ s^{-1}$ )
Allen, 1800 UTC 7 Aug 1980	86.8	79.5	78.1	74.0
Gilbert, 0000 UTC 14 Sep 1988	83.0	76.3	74.5	71.7
Hugo, 0400 UTC 22 Aug 1989	71.7	59.8	64.5	61.8
Andrew, 0900 UTC 24 Aug 1992	83.6	76.7	75.2	74.0
Mitch, 1900 UTC 26 Oct 1998	80.8	74.8	72.7	69.5

**5. Conclusions**

An improved method of estimating the maximum surface wind speed in a tropical cyclone was developed from measurements of the maximum flight-level (at 2–4-km altitude) and SFMR-estimated surface wind speeds from 179 radial flight legs in 15 hurricanes since 1998. The advantage of the new SFMR-based regression method over the GPS sonde-based methods is that the SFMR actually samples the maximum surface wind speed along a radial flight leg while insufficient sondes are available to sample the maximum. The mean slant reduction factor (ratio of radial-leg maximum surface wind speed to maximum flight level wind speed,  $F_{rmx}$ ) was 0.83 with a standard deviation of 9%. Azimuthal variability was found with larger values (to 0.89) in the left-front quadrant and weaker values (to 0.79) in the right-rear quadrant. The mean  $R_{mxs}$  was located at 0.875  $R_{mxf}$ , which is consistent with an outward tilt of the maximum wind radius with height. Several details apparent in the dataset were consistent with the Kepert (2001) and Kepert and Wang (2001) simulations of low-level jets in tropical cyclones, including 1) azimuthal variation in the reduction factor with higher values on the left [also reported by Franklin et al. (2003)]; 2) dependence of the reduction factor on storm motion speed, angular momentum, and inertial stability; and 3) a deficit of angular momentum at  $R_{mxs}$  compared to  $R_{mxf}$ . This strong consistency between theory and observations implies, to a high level of confidence, that these features are real. When the SFMR is not available, the regression method [Eq. (11)] is used in H\*Wind analyses (information online at [www.aoml.noaa.gov/hrd/data.html](http://www.aoml.noaa.gov/hrd/data.html)) to estimate the maximum surface wind speed from individual radial flight legs. Evaluations of the 90% rule (Franklin et al. 2003) and eyewall tilt

<sup>3</sup> In Table 6, the only HURDAT estimate influenced by the 90% rule was the reassessment of Hurricane Andrew.

TABLE 7. Evaluation of Eq. (11) using independent data (10 radial legs) from 2006 Hurricane Helene.

Reduction model	Bias (m s <sup>-1</sup> )	RMS error (m s <sup>-1</sup> )
SFMR based [Eq. (11)]	-0.7	3.0
0.8 at $R_{\text{mxf}}$	0.1	2.8
0.9 at $R_{\text{mxf}}$	4.5	5.4
Eyewall tilt at $R_{\text{mxf}}$	5.0	6.0
Mean $F_{\text{rmx}}$ (0.8346 $V_{\text{mxf}}$ )	1.6	3.3

(Dunion et al. 2003) flight-level wind reduction methods indicate overestimates of 4 and 8 m s<sup>-1</sup>, respectively, when applied to individual flight leg observations. For the purposes of estimating the maximum surface wind speed anywhere in the storm over an entire reconnaissance mission, Eq. (13) is appropriate. When applied to the maximum flight-level values observed over a flight mission, the 90% method shows a bias of 4.6 m s<sup>-1</sup>, which suggests a high bias in the recent historical record. Underestimates of intensity are suggested for some extreme storms in the historical record that occurred before the advent of GPS sondes or the SFMR. The regression method of Eq. (13) can be applied to reassess historical surface wind speed estimates during the era of aircraft reconnaissance, and is also applicable to calibration of satellite intensity estimation techniques.

*Acknowledgments.* We appreciate the efforts of our colleagues at HRD, NOAA's Aircraft Operations Center, and NHC, who persisted in exhaustive evaluations and calibrations of the SFMR during the 2005 Hurricane Field Program. Russell St. Fleur of the University of Miami Cooperative Institute for Marine and Atmospheric Studies helped assemble the eyewall GPS sonde dataset. We appreciate the suggestions of Jason Dunion and John Kaplan of HRD who provided internal reviews of the manuscript, as well as the three anonymous reviewers who made very helpful suggestions. This research was supported by the 2005 SFMR initiative, the NOAA 2006 Hurricane Supplemental, and the Army Corps of Engineers Hurricane Katrina Interagency Performance Evaluation Task Force.

## APPENDIX

### Derivation of Eqs. (4) and (5)

Equation (2) repeats Kepert's (2001) theoretical expression for the surface wind reduction factor  $F_r$  in terms of the dimensionless quantity  $\chi$  defined in (3). At the RMW, the radial gradient of  $V_G$  is zero and the Coriolis parameter is negligible, so  $I \approx \sqrt{2} V_G / R_{\text{MW}}$  and  $\chi = C_D \sqrt{M\sqrt{2}/K}$ , where  $M = V_G R_{\text{MW}}$  is the relative

angular momentum. Here,  $F_{\text{rmx}}$  can be written in terms of  $M$  by substituting this RMW value for  $\chi$  into (2). We then approximate  $F_{\text{rmx}}$  as a first-order Taylor series in  $\sqrt{M}$ :

$$F_{\text{rmx}}(\sqrt{M}) \approx F_{\text{rxm}}(\sqrt{M_0}) + (\sqrt{M} - \sqrt{M_0}) \partial F_{\text{rmx}} / \partial \sqrt{M} |_{M=M_0}.$$

Performing the differentiation, substituting in a typical eyewall value of  $M_0 = 2 \times 10^6 \text{ m}^2 \text{ s}^{-2}$  (e.g.,  $R_{\text{MW}} = 40 \text{ km}$ ,  $V_G = 50 \text{ m s}^{-1}$ ; see also Fig. 8) and reasonable values of  $C_D = 0.002$  and  $K = 50 \text{ m}^2 \text{ s}^{-1}$ , gives

$$F_{\text{rmx}} \approx 0.95 - 9.2 \times 10^{-5} \sqrt{M},$$

which is (4). The derivation of (5) is similar, except that the Taylor series is expanded in terms of  $M$  rather than  $\sqrt{M}$ . Comparison of the two approximations with (2) showed that the one in  $\sqrt{M}$  is a better approximation to (2) (not shown), but both are quite reasonable. Hence, it is appropriate to seek a linear relationship between  $F_{\text{rmx}}$  and either angular momentum or its square root at  $R_{\text{MW}}$ .

## REFERENCES

- Dunion, J. P., C. W. Landsea, S. H. Houston, and M. D. Powell, 2003: A reanalysis of the surface winds for Hurricane Donna of 1960. *Mon. Wea. Rev.*, **131**, 1992–2011.
- Eliassen, A., 1971: On the Ekman layer in a circular vortex. *J. Meteor. Soc. Japan*, **49**, 784–789.
- Emanuel, K. A., 1986: An air–sea interaction theory for tropical cyclones. Part I: Steady-state maintenance. *J. Atmos. Sci.*, **43**, 585–604.
- Frank, W. M., and E. A. Ritchie, 2001: Effects of vertical wind shear on the intensity and structure of numerically simulated hurricanes. *Mon. Wea. Rev.*, **129**, 2249–2269.
- Franklin, J. L., 2001: Guidance for reduction of flight-level observations and interpretation of GPS dropwindsonde data. NHC Internal Document. [Available from National Hurricane Center, 11691 SW 17th St., Miami, FL 33166-2149.]
- , M. L. Black, and K. Valde, 2003: GPS dropwindsonde wind profiles in hurricanes and their operational implications. *Wea. Forecasting*, **18**, 32–44.
- Haurwitz, B., 1935: The height of tropical cyclones and the “eye” of the storm. *Mon. Wea. Rev.*, **63**, 45–49.
- Hock, T. R., and J. L. Franklin, 1999: The NCAR GPS dropwindsonde. *Bull. Amer. Meteor. Soc.*, **80**, 407–420.
- Houze, R. A., Jr., and Coauthors, 2006: The hurricane rainband and intensity change experiment: Observations and modeling of Hurricanes Katrina, Ophelia, and Rita. *Bull. Amer. Meteor. Soc.*, **87**, 1503–1521.
- Jarvinen, B. R., C. J. Neumann, and M. A. S. Davis, 1988: A tropical cyclone data tape for the North Atlantic basin, 1886–1983: Contents, limitations, and uses. NWS Tech. Memo NWS NHC 22, 21 pp.
- Jones, S. C., 1995: The evolution of vortices in vertical shear. Part I: Initially barotropic vortices. *Quart. J. Roy. Meteor. Soc.*, **121**, 821–851.

- Kepert, J. D., 2001: The dynamics of boundary layer jets within the tropical cyclone core. Part I: Linear theory. *J. Atmos. Sci.*, **58**, 2469–2484.
- , 2006a: Observed boundary layer wind structure and balance in the hurricane core. Part I: Hurricane Georges. *J. Atmos. Sci.*, **63**, 2169–2193.
- , 2006b: Observed boundary layer wind structure and balance in the hurricane core. Part II: Hurricane Mitch. *J. Atmos. Sci.*, **63**, 2194–2211.
- , and Y. Wang, 2001: The dynamics of boundary layer jets within the tropical cyclone core. Part II: Nonlinear enhancement. *J. Atmos. Sci.*, **58**, 2485–2501.
- Khelif, D., S. P. Burns, and C. A. Friehe, 1999: Improved wind measurements on research aircraft. *J. Atmos. Oceanic Technol.*, **16**, 860–875.
- Landsea, C. W., J. L. Franklin, C. J. McAdie, J. L. Beven II, J. M. Gross, B. R. Jarvinen, J. P. Dunion, and P. Dodge, 2004: A reanalysis of Hurricane Andrew's (1992) intensity. *Bull. Amer. Meteor. Soc.*, **85**, 1699–1712.
- Montgomery, M. T., M. M. Bell, S. D. Aberson, and M. L. Black, 2006: Hurricane Isabel (2003): New insights into the physics of intense storms. Part I. *Bull. Amer. Meteor. Soc.*, **87**, 1335–1347.
- OFCM, 2007: National Hurricane Operations Plan. FCM-P12-2007, Office of the Federal Coordinator for Meteorological Services and Supporting Research, Washington, DC, 193 pp. [Available online at [www.ofcm.gov/nhop/07/pdf/entire-nhop07.pdf](http://www.ofcm.gov/nhop/07/pdf/entire-nhop07.pdf).]
- Olander, T., and C. Velden, 2007: The advanced Dvorak technique: Continued development of an objective scheme to estimate tropical cyclone intensity using geostationary infrared satellite imagery. *Wea. Forecasting*, **22**, 287–298.
- Powell, M. D., 1980: Evaluations of diagnostic marine boundary-layer models applied to hurricanes. *Mon. Wea. Rev.*, **108**, 757–766.
- , and P. G. Black, 1990: The relationship of hurricane reconnaissance flight-level wind measurements to winds measured by NOAA's oceanic platforms. *J. Wind Eng. Indust. Aerodyn.*, **36**, 381–392.
- , and S. H. Houston, 1996: Hurricane Andrew's landfall in south Florida. Part II: Surface wind fields and potential real-time applications. *Wea. Forecasting*, **11**, 329–349.
- , S. H. Houston, L. R. Amat, and N. Morisseau-Leroy, 1998: The HRD real-time hurricane wind analysis system. *J. Wind Eng. Indust. Aerodyn.*, **77/78**, 53–64.
- , T. A. Reinhold, and R. D. Marshall, 1999: GPS sonde insights on boundary layer wind structure in hurricanes. *Wind Engineering into the 21st Century*, A. Larsen, G. L. Larose, and F. M. Livesey, Eds., Taylor and Francis, 307–314.
- , P. J. Vickery, and T. A. Reinhold, 2003: Reduced drag coefficient for high wind speeds in tropical cyclones. *Nature*, **422**, 279–283.
- Rogers, R., and Coauthors, 2006: The Intensity Forecasting Experiment (IFEX): A NOAA multi-year field program for improving tropical cyclone intensity forecasts. *Bull. Amer. Meteor. Soc.*, **87**, 1523–1537.
- Schwendike, J., 2005: The boundary layer winds in Hurricanes Danielle (1998) and Isabel (2003). Diplomarbeit in Meteorology, Freie Universität, Berlin, Germany, 255 pp.
- , and J. A. Kepert, 2008: The boundary layer winds in Hurricanes Danielle (1998) and Isabel (2003). *Mon. Wea. Rev.*, **136**, 3168–3192.
- Shapiro, L., 1983: The asymmetric boundary layer flow under a translating hurricane. *J. Atmos. Sci.*, **40**, 1984–1998.
- Shaw, N., 1922: The birth and death of cyclones. *Geophys. Mem.*, **2**, 213–227.
- Uhlhorn, E. W., and P. G. Black, 2003: Verification of remotely sensed sea surface winds in hurricanes. *J. Atmos. Oceanic Technol.*, **20**, 99–116.
- , —, J. L. Franklin, M. Goodberlet, J. Carswell, and A. S. Goldstein, 2007: Hurricane surface wind measurements from an operational Stepped Frequency Microwave Radiometer. *Mon. Wea. Rev.*, **135**, 3070–3085.
- Walsh, E. J., and Coauthors, 2002: Hurricane directional wave spectrum spatial variation at landfall. *J. Phys. Oceanogr.*, **32**, 1667–1684.
- Willoughby, H. E., and M. B. Chelmon, 1982: Objective determination of hurricane tracks from aircraft observations. *Mon. Wea. Rev.*, **110**, 1298–1305.
- , J. A. Clos, and M. G. Shoreibah, 1982: Concentric eye walls, secondary wind maxima, and the evolution of the hurricane vortex. *J. Atmos. Sci.*, **39**, 395–411.
- , R. W. R. Darling, and M. E. Rahn, 2006: Parametric representation of the primary hurricane vortex. Part II: A new family of sectionally continuous profiles. *Mon. Wea. Rev.*, **134**, 1102–1120.
- Wright, C. W., and Coauthors, 2001: Hurricane directional wave spectrum spatial variation in the open ocean. *J. Phys. Oceanogr.*, **31**, 2472–2488.